



THE UNIVERSITY *of* EDINBURGH

Edinburgh Research Explorer

Are volcanic seismic b-values high, and if so when?

Citation for published version:

Roberts, NS, Bell, A & Main, I 2015, 'Are volcanic seismic b-values high, and if so when?' Journal of Volcanology and Geothermal Research. DOI: 10.1016/j.jvolgeores.2015.10.021

Digital Object Identifier (DOI):

[10.1016/j.jvolgeores.2015.10.021](https://doi.org/10.1016/j.jvolgeores.2015.10.021)

Link:

[Link to publication record in Edinburgh Research Explorer](#)

Document Version:

Peer reviewed version

Published In:

Journal of Volcanology and Geothermal Research

General rights

Copyright for the publications made accessible via the Edinburgh Research Explorer is retained by the author(s) and / or other copyright owners and it is a condition of accessing these publications that users recognise and abide by the legal requirements associated with these rights.

Take down policy

The University of Edinburgh has made every reasonable effort to ensure that Edinburgh Research Explorer content complies with UK legislation. If you believe that the public display of this file breaches copyright please contact openaccess@ed.ac.uk providing details, and we will remove access to the work immediately and investigate your claim.



Are volcanic seismic b -values high, and if so when?

Nick. S. Roberts^[1], Andrew F. Bell^[1], Ian G. Main^[1]

¹School of Geosciences, University of Edinburgh, James Hutton Road, Edinburgh, UK. EH9 3FE

Email: N.S.Roberts@sms.ed.ac.uk, a.bell@ed.ac.uk, ian.main@ed.ac.uk

1 Abstract

The Gutenberg-Richter exponent b is a measure of the relative proportion of large and small earthquakes. It is commonly used to infer material properties such as heterogeneity, or mechanical properties such as the state of stress from earthquake populations. It is 'well known' that the b -value tends to be high or very high for volcanic earthquake populations relative to $b=1$ for those of tectonic earthquakes, and that b varies significantly with time during periods of unrest. We first review the supporting evidence from of 34 case studies, and identify weaknesses in this argument due predominantly to small sample size, the narrow bandwidth of magnitude scales available, variability in the methods used to assess the minimum or cut-off magnitude M_c , and to infer b . Informed by this, we use synthetic realisations to quantify the effect of choice of the cut-off magnitude on maximum likelihood estimates of b , and suggest a new work flow for this choice. We present the first quantitative estimate of the error in b introduced by uncertainties in estimating M_c , as a function of the number of events and the b -value itself. This error can significantly exceed the commonly-quoted statistical error in the estimated b -value, especially for the case that the underlying b -value is high. We apply the new methods to data sets from recent periods of unrest in El Hierro and Mount Etna. For El Hierro we confirm significantly high b -values of 1.5-2.5 prior to the 10 October 2011 eruption. For Mount Etna the b -values are indistinguishable from $b=1$ within error, except during the flank eruptions at Mount Etna in 2001-2003, when $1.5 < b < 2.0$. For the time period analysed, they are rarely lower than $b=1$. Our results confirm that these volcano-tectonic earthquake populations can have systematically high b -values, especially when associated with eruptions. At other times they can be indistinguishable from those of tectonic earthquakes within the total error. The results have significant implications for operational forecasting informed by b -value variability, in particular in assessing the significance of b -value variations identified by sample sizes with fewer than 200 events above the completeness threshold.

Keywords: b -value; volcano; seismology; completeness magnitude

31 2 Introduction

32 Volcanic earthquakes provide insight into physical processes acting at volcanoes, such as the
33 mechanisms of deformation of the volcanic edifice and magma accumulation, and statistical analysis
34 of earthquake catalogues are a key component of eruption forecasting methods (McNutt, 1996).
35 Increased rates of earthquakes are a primary indicator of volcanic unrest, and changing locations of
36 earthquake hypocentres can be used to map magma migration (Wiemer and Wyss, 2002). The
37 frequency-magnitude distribution (FMD) of volcanic earthquakes can provide insight into the state of
38 stress or material properties, and are a key component of most studies of volcanic seismicity.

39 Where the catalogue is completely reported, the FMD, commonly takes the form of a Gutenberg-
40 Richter (GR) relation (Gutenberg and Richter, 1954):

$$\log(N) = a - bM, \quad (1)$$

41 where N is the total number of earthquakes of magnitude equal to or greater than M , and a and b are
42 real, positive constants characteristic of the specific catalogue. The parameter a is the logarithm of
43 the number of earthquakes with $M \geq 0$, and is thus a measure of the seismicity rate of the region. The
44 b -value represents the relative proportion of large and small events in the catalogue. It is best
45 calculated or inferred using the maximum likelihood method (Aki, 1965), now used almost universally
46 in earthquake seismology (Mignan and Woessner, 2012). Other methods such as a least squares fit of
47 the data to equation 1 are known to produce a biased estimate (Naylor et al., 2010). In addition, if the
48 bandwidth of data is narrow, or equivalently the sample is small, then it is easy to overestimate the
49 underlying b -value (Main, 2000). Finally, the b -value may also be biased due to incorrect identification
50 of the threshold for complete reporting, denoted M_c here (Mignan and Woessner, 2012). These and
51 other sources of bias introduce an epistemic error to any inference from the data. In principle this
52 should be accounted for in addition to the aleatory uncertainties inferred from the random error
53 associated with measurement or statistical fluctuation in the data, but it is often neglected in studies
54 of volcanic earthquake populations.

55 The Gutenberg-Richter form of the distribution holds, at least for small and intermediate events across
56 a remarkable range of sizes and loading conditions, from laboratory experiments to volcanic and
57 tectonic earthquakes (Main, 1996). In controlled laboratory tests, seismic b -values commonly change
58 systematically with respect to a variety of controlling factors. These include the degree of material
59 heterogeneity (Mogi, 1962), the level of applied stress (Scholz, 1968), the degree of stress
60 concentration, i.e. the stress intensity normalised to the fracture toughness (Meredith and Atkinson,
61 1983), the chemical reactivity of the pore fluid (Meredith and Atkinson, 1983), and the pore fluid
62 pressure (Sammonds et al., 1992). In nature other factors that affect the b -value systematically include
63 the earthquake focal mechanism (Schorlemmer et al., 2005), the depth (Mori and Abercrombie, 1997),

64 and the degree of coupling or strain partition between seismic and aseismic deformation at plate
65 boundaries (Mazzotti et al., 2011).

66 The b -value for tectonic earthquakes, using best practice and large regional or global data sets, is
67 commonly reported as taking values near unity (Frolich and Davis, 1993). In contrast the reported b -
68 values from published studies of earthquake populations associated with volcanic unrest are
69 commonly reported as being significantly higher than this, allowing for the random error expected for
70 a b -value of unity (described in more detail below). The main question we address here is whether this
71 difference is real or, at least to some extent, an artefact of the known sources of bias described above.

72 To examine this question we first use synthetic data to explore the effect of various factors on the
73 estimated b -value, denoted \tilde{b} , and the underlying b -value, henceforth denoted b . Uncertainties in \tilde{b}
74 at one standard deviation, denoted $\sigma_{\tilde{b}}$, are estimated using the method of Shi & Bolt (1982), which
75 correctly reflects the (approximately) Poisson ‘counting errors’ expected from sampling a whole
76 number of events (Greenhough and Main, 2008). The advantage of using synthetic data is that we can
77 distinguish between the random error $\sigma_{\tilde{b}}$, and the systematic error or bias $\tilde{b} - b$, or equivalently to
78 errors of precision and accuracy respectively. We show how both depend intrinsically on the sample
79 size. First we determine an optimum method of estimating the cut-off magnitude of complete
80 reporting of events, M_c , for catalogues of different sizes, and then propose a formal workflow for the
81 estimation of M_c . The proposed workflow is then applied to two volcanic seismic catalogues at Mount
82 Etna and El Hierro as important examples of recently-active volcanic systems to address the questions:
83 (a) are the b -values higher than 1? And (b) do they vary with time significantly outside the estimated
84 margins of error? For these examples, b is remarkably stationary and similar to (~ 1) or only somewhat
85 larger (1-1.5) than to those of tectonic earthquakes, except for specific transients where the b -value
86 can be significantly greater than background at 95% confidence. The results presented here will
87 provide greater confidence in identifying statistically-significant variations in b -value, and in identifying
88 physical causes for this variability.

89 3 Review and synthesis of previous studies

90 In this section we extend the review of McNutt (2005), who summarised reported b -values and
91 associated parameters such as source depth from 13 different volcanoes around the world. This review
92 includes b -values as high as 3 in one case (McNutt, 2005). In Table 1 we extend this study to 21
93 volcanoes, and include a wider range of associated parameters, including: the number of events; the
94 range of magnitudes used in the analysed catalogues; the methods used to calculate the completeness
95 magnitude and fit the b -value; and the range of b -values reported in each study, including a typical
96 value. Multiple studies use several methods for analysing b -value variations and thus the results are

97 reported separately in Table 1, giving 34 separate results for comparison in this new synthesis.
98 Information on all the different fields of data could not be found in all cases, e.g. how the threshold
99 magnitude was estimated, resulting in some blank entries in Table 1.

100 The maximum reported b -values range between 1.4 and 3.5, with a peak at $b=1.7$ (Figure 1c). From
101 Figures 1b there is no clear dependence on the magnitude and b -value. Bonnet et al. (2001) also found
102 there was no direct dependence of the scaling exponent for fracture length on the scale of observation
103 and that no significant trends could be determined in the type of faulting (Bonnet et al., 2001).

104 Figure 1 shows the distribution of b -values compared to the other variables in the study. There are no
105 clear trends with depth (Figure 1a) or magnitude range or size (Figure 1b). However, there is a weak
106 decreasing trend in the b -value as the number of events in the sample, N , increases (Figure 1c). The
107 data only spans from 10 to 300 events covering just over one magnitude unit, with over half, (16 of
108 25) of the studies using catalogues with either 50 or 100 events. One further study (Ibanez et al., 2012)
109 containing 7000 events reports a relatively high b -value of 1.57 that does not follow this trend.
110 However, this study - and many others cited in Table 1 - use the Least Squares method to fit b or to
111 check the results of the maximum likelihood estimation, introducing a known source of potential bias
112 outlined in the introduction.

113 In summary this review has highlighted a significant variability in the reported values of b , and a
114 significant variability in the methods of analysis used in the different studies. Typical b -values are
115 usually in the range 1-1.2. They are never (for this list) less than one, and are occasionally very high
116 (up to 3.5). The variability is much larger than any systematic trends, except that the b -value tends to
117 decrease with increasing sample size. In this paper we use synthetically-generated data to address
118 some of the most important origins of this variability, in particular the choice of threshold magnitude
119 and the sample size.

120 **4 Methods for analysis of Frequency-Magnitude Distributions**

121 A variety of statistical methods have been used to model FMD's and to quantify whether those models
122 are consistent with the observed data. Most methods involve modelling the proportion of the
123 distribution above the completeness magnitude. Therefore there is a strong inter-dependence
124 between estimates of the completeness magnitude and values of parameters of prospective FMD
125 models. In this section we summarise the current methods used to address this problem.

126 **4.1 Gutenberg-Richter parameters**

127 There is a well-established literature that describes the merits of different statistical methodologies
128 for FMD analysis. Methods involving regression on cumulative frequencies, or using least-squares

129 regression, are known to give biased estimates of the b -value (Naylor et al., 2010) as they are known
 130 to give disproportionate weighting to higher magnitude events (Ghosh et al., 2008). The maximum
 131 likelihood technique has become standard in seismic hazard analysis (Mignan and Woessner, 2012).
 132 The data are assumed to be exponentially distributed (as in eq. 1) and the maximum possible
 133 magnitude is assumed to be at infinity (Aki, 1965). Physically, earthquakes must have a finite maximum
 134 size dependent on the size and strain limits within the Earth, but M_{max} is not well constrained by global
 135 data (Main et al., 2008; Holschneider et al., 2014). The maximum likelihood method weights each
 136 event equally and correctly allows for error structure of the data: in frequency data in the form of a
 137 Poisson distribution (Naylor et al., 2010). Formally, the maximum likelihood estimate of the b -value is:

$$\tilde{b} = \frac{\log_{10} e}{\bar{M} - (M_c - \Delta M/2)} \quad (2)$$

138 where \tilde{b} is the estimate of the b -value, \bar{M} is the mean magnitude, M_c is the completeness magnitude,
 139 and ΔM is the magnitude bin size of the histogram (Aki, 1965). Aki also showed the uncertainty on
 140 this estimate at one standard deviation (67% confidence) can be approximated to:

$$\sigma_{\tilde{b}} = \frac{\tilde{b}}{\sqrt{N_c}} \quad (3)$$

141 Where N_c is the number of events in the complete part of the catalogue, or 1.96 times this value at
 142 95% confidence.

143 A summary study by Marzocchi & Sandri, (2003), tested two further improvements on this estimation
 144 of b using binned magnitudes, equation (4) (Bender, 1983), and an improved uncertainty estimate (eq.
 145 5) (Shi and Bolt, 1982; Marzocchi and Sandri, 2003):

$$\tilde{b} = \frac{1}{\ln 10[\hat{\mu} - (M_c - \Delta M)]} \quad (4)$$

$$\sigma_{\tilde{b}} = 2.30\tilde{b}^2 \sqrt{\frac{\sum_{i=1}^N (M_i - \hat{\mu})^2}{N_c(N_c - 1)}}$$

146 where $\hat{\mu}$ is the average magnitude of the sample, and ΔM is the binned magnitude width. The b -value
 147 is relatively insensitive to the upper magnitude cut-off, so assuming an infinite cut-off in deriving
 148 equations (3) and (5) does not introduce a significant bias. However, in both cases the quoted error is
 149 formally conditional on the choice of M_c , which in practice must be estimated. This introduces an
 150 implicit source of bias that can be positive or negative. In this paper we will demonstrate that this
 151 additional source of uncertainty is comparable to or can greatly exceed the estimates from equations
 152 (3) or (5).

153 4.2 Calculating the completeness magnitude

154 Most studies apply a lower threshold or cut-off magnitude, M_c , above which the catalogue can be
155 regarded as completely recorded (Wiemer and Wyss, 2000). M_c is the lowest magnitude at which 100
156 per cent of earthquakes in a space-time volume are detected (Rydelek and Sacks, 1989; Woessner and
157 Wiemer, 2005; Mignan and Woessner, 2012). Earthquakes with smaller magnitudes are less likely to
158 be completely reported when their amplitude becomes smaller than that of the ambient noise. This
159 introduces a high-pass filter to the FMD, which could in principle be modelled and fitted to the data.
160 However, this is rarely (if ever) done explicitly. In practice most studies assume M_c is the magnitude
161 at which the log(cumulative frequency)-magnitude curve departs from a linear trend of eq. 1. There
162 are three main techniques commonly used to estimate this magnitude, namely the Maximum
163 Curvature (MaxC) method, the Goodness-of-Fit test (GFT) (Wiemer and Wyss, 2000) and b -value
164 stability (BVS) method (Cao and Gao, 2002).

165 The MaxC method calculates the highest value of the first derivative of the cumulative frequency-
166 magnitude curve. In practice this matches the frequency-magnitude bin with the highest number of
167 events (Figure 2a). The main limitation of this method is that it will systematically underestimate M_c
168 unless there is a sharp transition between the incomplete and complete portion of the catalogue, as
169 illustrated in Figure 2a.

170 The GFT method calculates M_c by comparing the observed FMD with a synthetic one. The best-fit
171 distribution is calculated for trial cut-off magnitudes using the maximum-likelihood estimates of a - and
172 b -values of the observed dataset. The residuals between the data and the best fit distribution are then
173 calculated as a function of cut-off magnitude (Figure 2b). The completeness threshold, M_c , is selected
174 as being the first magnitude above which the residual between the synthetic straight line fit model
175 and observed data falls within a 95% confidence window. If 95% confidence cannot be obtained then
176 a 90% confidence window can be used as a compromise. This method tends to give systematically low
177 values for M_c although not as low as the MaxC method (Wiemer and Wyss, 2000).

178 The BVS method simply evaluates the estimated b -value as a function of the cut-off magnitude. The
179 assumption here is that \tilde{b} will initially increase as the cut-off magnitude increases, until the cut-off
180 magnitude equals M_c after which \tilde{b} will stabilise. The inferred b -value is deemed to have stabilised
181 once the average \tilde{b} for the five successive cut-off magnitudes falls within error of the selected cut-off
182 magnitude (Figure 2c). The BVS method tends to have high M_c values relative to other methods
183 (Woessner and Wiemer, 2005) and consequently higher \tilde{b} values.

184 5 Results for Synthetic catalogues

185 5.1 Generating synthetic catalogues

186 We now evaluate which of the three methods for calculating the M_c is the most accurate and reliable,
187 by generating synthetic catalogues with known M_c and b -value, but different forms of the cut off
188 below M_c . As a benchmark check we first generated synthetic data to determine \tilde{b} and $\sigma_{\tilde{b}}$ for $b=1$ and
189 $b=2$ as a function of the complete sample size N_c , conditioned on an exact value for M_c . This provided
190 a good match to Fig. 1a,b of Marzocchi and Sandri (2003). However, in reality M_c is not known
191 independently a priori. Ideally we would hope the incremental FMD would have a sharp and easily
192 distinguishable peak at M_c , defining the lower limit of the complete catalogue (Figure 3a). In reality
193 the peak of the distribution is often curved and much broader due to the complexity of the signal to
194 noise ratio at the recording stations, and of locating and calculating magnitudes for small events, so
195 defining M_c can be much more challenging (Figure 3b). This introduces an additional source of
196 uncertainty that is the prime focus of the current paper.

197 To test each of the three methods, we use two end-member scenarios. The first has a sharp peak
198 (Figure 3a) and the second a broader peak (Figure 3b). Both catalogues have M_c set to 1.0. The
199 complete part of both catalogues was created by randomly generating individual events from an ideal
200 parent Gutenberg-Richter law distribution with a b -value of 1.0. For the sharp-peaked distribution the
201 incomplete part of the catalogue was generated using a filter with a linear slope of 3, for values below
202 $M_c=1.0$ decaying to zero probability at $M=0$. For the broad-peaked distribution a GR distribution was
203 used to generate events all the way down to $M=0$. The probability function shown in Figure 3c was
204 then applied as a filter to remove events below the known threshold $M_c=1.0$, until the required
205 number of events were left in the complete catalogue.

206 To examine the role of catalogue size, catalogues were generated with a complete size of 50, 100, 200,
207 500, 1000 and 5000 events. Finally the b -value was varied from a typical tectonic value of 1.0 to a
208 significantly high b -value of 2.0, to test whether each method can reliably calculate M_c and inferred b -
209 values for the case that the underlying b -value is high.

210 For each catalogue size, b -value, and distribution shape; 100 catalogue were iteratively generated, and
211 the estimated M_c and b -values determined using the different methods described in section 4. A bin
212 size ΔM of $0.1M$ is used throughout. Figure 3 shows both the average catalogue (solid line) and the
213 spread of the outcomes associated with the finite sample size (dashed lines).

214 5.2 Synthetic Results

215 5.2.1. Sharp-peaked distribution

216 In this case the simulations of Figure 4 demonstrate that the MaxC method performs the best in terms
217 of calculating M_c , closely followed by the BVS method. The GFT performs adequately for $N_c=5000$ but
218 fails when $N_c=50$ as for over 90% of the catalogues b is not even calculated correctly within ± 1.0 of the
219 known value. When $b=1$ and $N_c=5000$, MaxC and BVS both correctly lead to a correct calculation of b
220 with <0.01 error.

221 5.2.2. Broad-peaked distribution

222 Figure 5 shows histograms of the best estimates of M_c for the three methods, for different catalogue
223 sizes and b -values, for the case of the broad-peaked distribution. When $N_c=50$ for both $b=1$ and $b=2$,
224 MaxC and BVS both systematically underestimate M_c , because very few events have a greater
225 magnitude than $M_c=1.0$ (Figure 6). Both MaxC and BVS methods give results with some scatter,
226 centred on $b=1$, but several iterations had significantly higher b -values of 2 or above. Both methods
227 perform poorly when $b=2$, as there too few events in the catalogue, with median values of $\tilde{b}\approx 1.5$. The
228 GFT over-estimates M_c when $b=1$ but appears to give a reasonable estimate when $b=2$. However, the
229 95% confidence is only reached when M_c is very close to the maximum magnitude and thus the
230 complete catalogue size is very small. This results in the inferred b -values being very high for both $b=1$
231 and $b=2$.

232 When $N_c=5000$ it becomes apparent that MaxC is not a good method for broad-peaked distributions.
233 For $b=1$, M_c is heavily underestimated, with a median value of $M_c=0.4$, and resulting \tilde{b} -values all less
234 than $b=1$. These underestimates are amplified when $b=2$ with median values of $M_c=0.4$ and $\tilde{b}\approx 1.3$. The
235 GFT performs much better for both $b=1$ and $b=2$ however it gives a conservative estimate for both.
236 The BVS method performs the best for a broad-peaked distribution, giving only a slightly conservative
237 estimate of M_c with a median value of $M_c=0.9$ for $b=1$ and $b=2$. The BVS method returns the correct
238 $\tilde{b}=1.0$ in over 80 iterations. The median value for $b=2$ is also approximately correct, however there is
239 a very broad range of results with a slight skew towards values higher than $b=2.0$. This is a very large
240 catalogue and the BVS method is clearly the best when $b=2$. Our results show that it is intrinsically
241 more difficult to calculate high b -values, however it is possible to find an estimate with a correct
242 median value with the BVS method, albeit with a large spread in \tilde{b} .

243 5.2.3. Comparison of method performance

244 For a sharp-peaked distribution the MaxC method correctly calculates M_c the highest proportion of
245 times for both high and low b -values. This outcome is not surprising as the MaxC method finds the
246 magnitude bin with the highest number of events that, trivially, is the M_c set by the parent distribution.

247 The BVS method performs almost as well as the MaxC method for low b -values, but with higher b -
248 values the method returns too high estimates of M_c . However, as long as for larger catalogue sizes the
249 BVS method continues to return good estimates of the b -value. The GFT method does not work with
250 small catalogues as the 95% confidence threshold is only reached when the M_c is very close to the
251 maximum magnitude event, therefore there are a minimal number of earthquakes left in the
252 catalogue, and thus the uncertainty is very large. For larger catalogues GFT performs much better.
253 However for both $b=1$ and $b=2$, using the GFT-calculated value of M_c results in fewer correct
254 calculations of \tilde{b} than the MaxC and BVS methods. Therefore we consider it to be the least-well
255 performing method. For $b=2$ the steeper slope of the complete catalogue leads to a larger spread of
256 calculated \tilde{b} -values for all three methods than for $b=1$. This is due to the random scattering of data
257 due to sampling which has a greater influence on the FMD at high b compared to low b -values, and is
258 not inherently linked to any of the methodologies.

259 Figure 7 and Figure 8 compare the performance of the different methods for the case of a broad-
260 peaked distribution, using the mean and standard deviations of \tilde{b} calculated from the data in Figure 6.
261 For both b -values the GFT method does not reliably calculate M_c , resulting in a biased estimate of the
262 b -value. For $N_c \leq 500$ the correct b -value is calculated within the statistical error, but the distribution is
263 heavily skewed towards high b -values, meaning that this method performs sub-optimally for these
264 small catalogue sizes. However for larger catalogues ($N_c=1000$ & 5000) the GFT method does calculate
265 accurate b -value estimates for both $b=1$ and $b=2$. The MaxC method returns a systematically-low
266 estimate of M_c for all catalogue sizes, resulting in under-estimates of the b -value for both $b=1$ and
267 $b=2$. We conclude that it is not an appropriate method for calculating M_c for a broad-peaked
268 distribution.

269 The estimates of M_c returned by the BVS method increase in accuracy with catalogue size. For $N_c \geq 200$
270 the BVS method correctly calculates M_c within the 95% confidence limits for both $b=1$ (Figure 7) and
271 $b=2$ (Figure 8). When $b=1$ and the catalogue size is $N_c \geq 200$, the 95% confidence spread around the
272 true b -value is very small, ± 0.25 . Using the BVS method with smaller catalogue sizes can result in b -
273 value estimates as high as 2 even with $b=1$ (Figure 7). This observation suggests that care must be
274 taken to not over-interpret high b -values calculated for small catalogue sizes. For $b=2$, the standard
275 deviation of results is independent of catalogue size at about ± 0.75 . However, the median and mean
276 of the \tilde{b} -value estimates tend towards the parent $b=2$ as catalogue size increases. Again for $N_c \geq 200$
277 for $b=2$ the BVS method estimates \tilde{b} to within 95% confidence.

278 In terms of defining a threshold minimum complete catalogue size, when $N_c \geq 500$ our results show
279 both $b=1$ and $b=2$ can be estimated accurately and precisely (Figure 7). For $N_c=100$ the statistical error
280 in estimating $b=1$ is large, indicating a lack of precision, and for $b=2$ the average and median values are

281 significantly below 2, indicating a residual bias. However, a threshold of 500 for completely-reported
282 events is a relatively large number for many practical applications. From the results in Figure 7, a
283 pragmatic choice of $N_c=200$ is an acceptable threshold for a trade-off between accuracy, precision,
284 and realistic catalogue size.

285 **5.3 A proposed workflow for the calculation of M_c**

286 Informed by this analysis, we propose a workflow for analysing the FMD of volcanic earthquake
287 catalogues (Figure 9). As discussed above, we considered that the minimum catalogue size for reliable
288 estimation of the b -value is $N_c=200$.

289 First, M_c is estimated using each of the MaxC, GFT and BVS methods. If all three M_c estimates agree
290 within ± 0.1 , the FMD can be modelled by a sharp-peaked distribution, and so the MaxC estimate of
291 M_c should be used. If the b -value calculated using this M_c has an error of $\leq \pm 0.25$ it should be
292 considered to be reliable. An error of $> \pm 0.25$ makes it difficult to interpret the b -value and may indicate
293 an unreliable estimate of M_c .

294 If the three estimates of M_c vary by ≥ 0.1 , or the b -value calculated from the MaxC estimate of M_c is
295 ≥ 0.25 , we recommend that the BVS method should be used. If the resulting b -value has an error of
296 ≤ 0.25 it should be considered to be reliable. If this is not the case, the GFT analysis should be used. If
297 a b -value with an error of ≤ 0.25 cannot be obtained using any of the 3 methods, we argue that the
298 catalogue is too small for reliable FMD analysis. If the complete catalogue has over 5000 events and
299 the b -value uncertainty is still too high, it is likely that the FMD is not consistent with an underlying
300 Gutenberg-Richter distribution.

301 For the analysis of variations in FMDs, a large volcanic earthquake catalogue can be split on the basis
302 of spatial or temporal windows, and this workflow applied to each sub-catalogue in turn. However,
303 the same minimum complete catalogue size and reliability criteria rules apply to sub catalogues too.

304 **5.4 Error introduced from the completeness magnitude**

305 We now use the workflow of Figure 9 to consider the relative effect of M_c estimation for catalogues
306 of different size on the accuracy and precision of the estimate of \tilde{b} for the case of a broad-peaked
307 distribution. Figure 10 shows a histogram of the \tilde{b} for 100 catalogue realizations with $b=2$, along with
308 examples of its standard deviation $\sigma_{\tilde{b}}$ estimated from equation 5. \tilde{b} is beyond 1 standard deviation of
309 b in more than 1/3 of the cases, indicating a significant epistemic error in the estimation. We show in
310 this section that this is due to the bias $\tilde{b} - b$ in the finite-sized sample. The error due to calculating M_c
311 for individual realisations is illustrated as a blue bar at one standard deviation in Figure 9. The median
312 \tilde{b} is close to the true value (the central blue dot is near the vertical dashed line), so the residual bias
313 due to estimating M_c is near zero for a large population of trials. However, the standard deviation in

314 the error due to Mc is much larger than the average statistical error for similar b -values (the black
315 error bars).

316 To quantify this error in the general case, we ran many simulations for different values of b and N_c ,
317 with the results shown in Figure 11. Figure 11a shows the average statistical error from equation (5),
318 Figure 11b the average error in \tilde{b} due to propagating uncertainties in estimating Mc as illustrated by
319 the blue horizontal error bar in Figure 10, and Figure 11c the ratio of the two. The ratio was calculated
320 5 times for each of 15 catalogue sizes between 50-5,000 events and b -values of 0.5, 1.0, 1.5, 2.0 & 3.0,
321 with the average value indicated by the colour scheme in Figure 11. The ratio varies between 1.2 and
322 a factor 14 or so for the range studied, implying that the sample bias error is always greater than, and
323 often much greater than the estimated statistical uncertainty in \tilde{b} from equation (5). This finding
324 means that the statistical error commonly used on its own to quantify the \tilde{b} -value uncertainty is not
325 an adequate description of the total error, though it approaches the total error for large numbers of
326 events and low underlying b -values. In Figure 11c the ratio can reach an order of magnitude for $b > 2$
327 and event numbers above 1000. This is because the statistical error $\sigma_{\tilde{b}}$ is very small when N_c is large.
328 However the sample bias also increases with N_c for high b . This somewhat counter-intuitive result is
329 because the magnitude range over which Mc can be calculated is much smaller at low N_c than at high
330 N_c , so the uncertainty is bounded to a greater degree at low N_c , and hence reduces at low N_c . The
331 template of Figure 11c can be used empirically to determine a more appropriate error for b -value
332 estimation.

333 **5.5 Application to volcanic catalogues**

334 We apply our proposed workflow to earthquake catalogues for Mount Etna volcano, Sicily (Murru et
335 al., 1999; Murru et al., 2005; Murru et al., 2007) and El Hierro volcano, Canary Islands (Ibanez et al.,
336 2012; López et al., 2012; Becerril et al., 2013; Marti et al., 2013; García et al., 2014) to test the reliability
337 of any previously reported variations in b -values. This is simply to compare results from the proposed
338 workflow to previous volcanic b -value's and not to make any interpretation about the behaviour of
339 the volcanos.

340 We analyse the Instituto Geográfico Nacional (IGN) earthquake catalogue for El Hierro between July
341 2011 and December 2013, a period associated with significant seismic activity associated with magma
342 emplacement, and including a submarine eruption that began on 10th October 2011 (Ibanez et al.,
343 2012; López et al., 2012). The catalogue contains over 20,000 events, and so it is possible to subdivide
344 it into several phases to analyse b -value variations. Figure 12 shows how each phase is defined by
345 changes in event rate, with the first three phases following the scheme of Ibanez et al. (2012). The
346 start of each phase is defined as midnight at the start of the selected day, however, if necessary the
347 resolution of the boundaries can be increased as most catalogues give event time to the nearest

348 second. All phases have over 200 events at or above M_c , thus the catalogues should be large enough
349 to calculate reliable \tilde{b} -values following the synthetic analysis. At this stage the catalogue is simply
350 divided temporally, so earthquakes may originate from different portions of the volcanic edifice.
351 Should this occur, the b estimate may represent an average between sub-catalogues representative
352 of different processes or stress conditions.

353 The results of applying our proposed workflow to the El Hierro catalogue are shown in Figure 12. These
354 show a very high b -value of $\tilde{b}=2.39\pm 0.10$ before the onset of the eruption, followed by a fluctuating \tilde{b} -
355 value between 1-1.5 for the remainder of the catalogue. \tilde{b} -value uncertainties are determined using
356 equation 5. The \tilde{b} -value is always above 1 within these statistical errors. These results are similar to
357 those of Ibanez et al. (2012), who reported a b -value before the eruption of 2.25 ± 0.05 followed by
358 values of $b=1.34\pm 0.04$ and $b=1.12\pm 0.01$ for the second and third phases respectively (Ibanez et al.,
359 2012). However, the Ibanez study used the 90% Goodness-of-fit method to estimate M_c , and least-
360 squares regression to estimate b . The M_c values they report are significant under-estimates, and this
361 means that the biased least-squares b -value estimates are, coincidentally, close to the values reported
362 here.

363 We also analyse the Istituto Nazionale di Geofisica e Vulcanologia (INGV) earthquake catalogue for Mt
364 Etna between January 1999 and December 2014. This catalogue spans several eruptive episodes,
365 including the 2001 and 2002-03 flank eruptions and more recent paroxysmal activity at the new South
366 East Crater. The catalogue contains 8000 events, with an event rate that is more stable through time
367 than the El Hierro catalogue (Figure 12 and Figure 13). We divide the catalogue into 10 sub-phases on
368 the basis of changes in earthquake rate, with each phase ideally containing between 200-5000 events.

369 Figure 13 shows the \tilde{b} -values calculated for Mt Etna using our proposed workflow. During the 2001
370 and 2002-03 flank eruptions the \tilde{b} -value is 1.5 or greater. However from the end of the 2002-03 flank
371 eruption, the \tilde{b} -value appears to have stabilised at 1.0 ± 0.2 . Murru et al. (2007) analysed the spatial
372 distribution of the b -value at Mt Etna between 1999 and 2005 and found an average of approximately
373 1.5, with an increase in average b -value with depth from $b=1.2$ to $b=1.9$.

374 Although the \tilde{b} -values for Mt Etna from 2004 onwards are close to 1.0 and there is no systematic trend
375 in values, the \tilde{b} -values do not encompass $b=1$ within error for over half of the sub-phases in Figure 13.
376 As the Shi & Bolt \tilde{b} -value uncertainty (eq. 5) defines one standard deviation error in the \tilde{b} -value we
377 would expect 68% of the calculated b -values to capture $b=1$ within error if the underlying b -value is
378 stationary. We might then conclude that the hypothesis that $b=1$ can be rejected at this confidence
379 level. However, we have shown that the total error, including sample bias, can be significantly
380 underestimated in Figure 11.

381 Accordingly we now apply the contour plot for the error multiplication values in Figure 11c to estimate
382 a more realistic total error for our calculated b -value. For the 2011-13 El Hierro catalogue (Figure 14a)
383 the high b -values at the start of the catalogue now have dramatically increased errors, and 3 of the 6
384 following b -values that sat between $1 > \tilde{b} > 1.5$ now lie within 1 standard deviation error around $b=1.0$.
385 Using the Shi & Bolt uncertainty for the 2004-2014 Etna catalogue, the estimated \tilde{b} -values for only 2
386 of 10 phases (20%) lie within one standard deviation of $b=1.0$. However, once the modified error is
387 applied to the catalogue (Figure 14b), the estimated \tilde{b} -value for 6 of the 10 phases (60%) lie within 1
388 standard deviation of $b=1.0$. The high b -values associated with the 2001 and 2002-03 flank eruptions
389 also increase in error and could be consistent with b -value of no more than 1.5. The b -values for 3 of
390 the 10 phases do not lie within 2 standard deviations of $b=1$ using the modified error. Therefore it
391 would be hard to reject the hypothesis that b is a constant near unity for these phases, except at
392 marginal significance.

393 6 Conclusions

394 The almost axiomatic inference that b -values are systematically higher for volcanic earthquakes is
395 based on data and methodology that are often insufficient to address the question, notably the very
396 small sizes of the samples used, the methods of parameter estimation and the different methods used
397 to infer the completeness magnitude M_c . The Maximum Curvature method is simple, and can be used
398 when a catalogue has a sharp peak in the discrete data. Otherwise the b -value stability method is the
399 most favourable. If that does not generate a b -value with a standard error ≤ 0.25 the Goodness-of-Fit
400 method can be used as a third option. If a stable value of b cannot be obtained then the sample size
401 must be increased in space and/or time. Our results imply a pragmatic minimum of 200 events above
402 M_c is generally needed. From further simulations, we also recommend a minimum of 500 events when
403 dealing with raw incomplete catalogues before this workflow can be applied. This logic is captured in
404 a new workflow for estimating M_c . Even when this best practice is followed, there can be a significant
405 residual error from calculating M_c in a single sample. This is comparable to or much greater than the
406 statistical error, particularly for higher values of b . Nevertheless, when this is accounted for we
407 confirm b -values for the El Hierro catalogue are generally higher than 1 at a confidence level of 95%,
408 and may be significantly higher during eruptive phases. For Mount Etna the hypothesis $b=1$ can be
409 rejected for only two time intervals, one associated with a flank eruption. We conclude seismic b -
410 values can be high for volcanic earthquake populations, especially when associated with eruptive
411 phases. Otherwise they appear to be very close to those obtained for tectonic earthquakes at the 95%
412 confidence level.

413

414 **7 Acknowledgements**

415 Nick Roberts is a NERC funded PhD student at the University of Edinburgh. We thank the Instituto
416 Geográfico Nacional and INGV Sezione di Catania for making the seismic catalogues for El Hierro and
417 Mount Etna respectively available, Mark Naylor for providing feedback on earlier drafts of the paper,
418 and three anonymous reviewers, and Jackie Caplan-Auerbach for improving the paper with their critical
419 feedback.

420

421

422 8 References

- 423 Aki, K., 1965. Maximum Likelihood Estimate of b in the Formula $\log N = a - bM$ and its confidence limits.
424 Bulletin of the Earthquake Research Institute, 43: 237-239.
- 425 Becerril, L., Cappello, A., Galindo, I., Neri, M. and Del Negro, C., 2013. Spatial probability distribution
426 of future volcanic eruptions at El Hierro Island (Canary Islands, Spain). Journal of Volcanology
427 and Geothermal Research, 257: 21-30.
- 428 Bender, B., 1983. Maximum likelihood estimation of b values for magnitude grouped data. Bulletin of
429 the Seismological Society of America, 73(3): 831-851.
- 430 Bonnet, E., Bour, O., Odling, N.E., Davy, P., Main, I., Cowie, P. and Berkowitz, B., 2001. Scaling of
431 fracture systems in geological media. Review of Geophysics, 29(3): 347-383.
- 432 Bridges, D.L. and Gao, S.S., 2006. Spatial variation of seismic b -values beneath Makushin Volcano,
433 Unalaska Island, Alaska. Earth and Planetary Science Letters, 245: 408-415.
- 434 Cao, A. and Gao, S.S., 2002. Temporal variation of seismic b -values beneath northeastern Japan island
435 arc. Geophysical Research Letters, 29(9): 1-3.
- 436 Centamore, C., Patane, G. and Tuve, T., 1999. Maximum entropy estimation of b values at Mt. Etna:
437 comparison with conventional least squares and maximum likelihood results and correlation
438 with volcanic activity. Annali Di Geofisica, 42(3): 515-528.
- 439 Farrell, J., Husen, S. and Smith, R.B., 2009. Earthquake swarm and b -value characterization of the
440 Yellowstone volcano-tectonic system. Journal of Volcanology and Geothermal Research, 188:
441 260-276.
- 442 Frolich, C. and Davis, S.D., 1993. Telesismic b values; Or, Much Ado About 1.0. Journal of Geophysical
443 Research, 98(No. B1): 631-644.
- 444 García, A., Fernandez-Ros, A., Berrocoso, M., Marrero, J.M., Prates, G., De la Cruz-Reyna, S. and Ortiz,
445 R., 2014. Magma displacements under insular volcanic fields, applications to eruption
446 forecasting: El Hierro, Canary Islands, 2011–2013. Geophys. J. Int.
- 447 Ghosh, A., Newman, A.V., Thomas, A.M. and Farmer, G.T., 2008. Interface locking along the subduction
448 megathrust from b -value mapping near Nicoya Peninsula, Costa Rica. Geophysical Research
449 Letters, 35(L01301).
- 450 Greenhough, J. and Main, I., 2008. A Poisson model for earthquake frequency uncertainties in seismic
451 hazard analysis. Geophysical Research Letters, 35.
- 452 Gutenberg, B. and Richter, C.F., 1954. Seismicity of the Earth, 2nd ed., 310.
- 453 Holschneider, M., Zoller, G., Clements, R. and Schorlemmer, D., 2014. Can we test for the maximum
454 possible earthquake magnitude? J. Geophys. Res. Solid Earth, 199: 2019-2028.

455 Ibanez, J.M., De Angelis, S., Diaz-Moreno, A., Hernandez, P., Alguacil, G., Posdas, A. and Perez, N., 2012.
456 Insights into the 2011-12 submarine eruption off the coast of El Hierro (Canary Islands, Spain)
457 from statistical analyses of earthquake activity. *Geophys. J. Int.*, 191: 659-670.

458 Jacobs, K.M. and McNutt, S.R., 2010. Using seismic b-values to interpret seismicity rates and physical
459 processes during the preeruptive earthquake swarm at Augustine Volcano 2005-2006. *USGS*
460 *Professional Paper*, 1769-3: 59-83.

461 Jolly, A.D. and McNutt, S.R., 1999. Seismicity at the volcanoes of Katmai National Park, Alaska; July
462 1995-December 1997. *Journal of Volcanology and Geothermal Research*, 93: 173-190.

463 López, C., Blanco, M.J., Abella, R., Brenes, B., Rodríguez, V.M.C., Casas, B., Cerdeña, I.D., Felpeto, A.,
464 Villalta, M.F., Del Fresno, C., García, O., García-Arias, M.J., García-Cañada, L., Moreno, A.G.,
465 Gonzalez-Alonso, E., Pérez, J.G., Iribarren, I., López-Díaz, R., Luengo-Oroz, N., Meletlidis, S.,
466 Moreno, M., Moure, D., Pablo, J.P., Rodero, C., Romero, E., Sainz-Maza, S., Domingo, M.A.S.,
467 Torres, P.A., Trigo, P., Villasante-Marcos, V., de Villalta, M.F. and de Pablo, J.P., 2012.
468 Monitoring the volcanic unrest of El Hierro (Canary Islands) before the onset of the 2011–2012
469 submarine eruption. *Geophysical Research Letters*, 39(13).

470 Main, I., 1996. Statistical Physics, Seismogenesis, and Seismic Hazard. *Review of Geophysics*, 34(4):
471 433-462.

472 Main, I., 2000. Apparent Breaks in Scaling in the Earthquake Cumulative Frequency-Magnitude
473 Distribution: Fact or Artifact? *Bulletin of the Seismological Society of America*, 90(1): 86-97.

474 Main, I.G., 1987. A characteristic earthquake model of the seismicity preceding the eruption of Mount
475 St. Helens on 18 May 1980. *Physics of the Earth and Planetary Interiors*, 49: 283-293.

476 Main, I.G., Li, L., McCloskey, J. and Naylor, M., 2008. Effect of the Sumatran mega-earthquake on the
477 global magnitude cut-off and event rate. *Nature Geoscience*, 1: 142.

478 Marti, J., Pinel, V., Lopez, C., Geyer, A., Abella, R., Tarraga, M., Blanco, M.J., Castro, A. and Rodriguez,
479 C., 2013. Causes and mechanisms of El Hierro submarine eruption (2011-2012) (Canary
480 Islands). *JGR*: 1-47.

481 Marzocchi, W. and Sandri, L., 2003. A review and new insights on the estimation of the b-value and its
482 uncertainty. *Annals of Geophysics*, 46(6): 1271-1282.

483 Mazzotti, S., Leonard, L.J., Cassidy, J.F., Rogers, G.C. and Halchuk, S., 2011. Seismic hazard in western
484 Canada from GPS strain rates versus earthquake catalog. *Journal of Geophysical Research*,
485 116(B12310): 1-17.

486 McNutt, S.R., 1996. Seismic Monitoring and Eruption Forecasting of Volcanoes: A Review of the State-
487 of-the-Art and Case Histories. 9-146.

488 McNutt, S.R., 2005. Volcanic Seismology. *Annual Review of Earth and Planetary Sciences*, 33(1): 461-
489 491.

490 Meredith, P.G. and Atkinson, B.K., 1983. Stress corrosion and acoustic emission during tensile crack
491 propagation in Whin Sill dolerite and other basic rocks. *Geophys. J. R. astr. Soc.*, 75(1): 1-21.

492 Mignan, A. and Woessner, J., 2012. Estimating the magnitude of completeness for earthquake
493 catalogs. *Community Online Resource for Statistical Seismicity Analysis*: 1-45.

494 Mogi, K., 1962. Magnitude frequency relations for elastic shocks accompanying fractures of various
495 materials and some related problems in earthquakes. *Bull. Earthquake Res. Inst. Univ. Tokyo*,
496 40: 831-853.

497 Mori, J. and Abercrombie, R.E., 1997. Depth dependence of earthquake frequency-magnitude
498 distributions in California: Implications for rupture initiation. *Journal of Geophysical Research*,
499 102: 15081-15090.

500 Murru, M., Console, R., Falcone, G., Montuori, C. and Sgroi, T., 2007. Spatial mapping of the *b* value at
501 Mount Etna, Italy, using earthquake data recorded from 1999 to 2005. *J. Geophys. Res.*,
502 112(B12303).

503 Murru, M., Montuori, C., Console, R. and Lisi, A., 2005. Mapping of the *b* value anomalies beneath Mt.
504 Etna, Italy, during July-August 2001 lateral eruption. *Geophysical Research Letters*,
505 32(L05309).

506 Murru, M., Wyss, M. and Privitera, E., 1999. The locations of magma chambers at Mt. Etna, Italy,
507 mapped by *b*-values. *Geophysical Research Letters*, 26(16): 2553-2556.

508 Naylor, M., Orfanogiannaki, M. and Hart, D., 2010. Exploratory data analysis: magnitude, space, and
509 time. *Community Online Resource for Statistical Seismicity*: 1-42.

510 Novelo-Casanova, D.A., Martinez-Bringas, A. and Valdes-Gonzalez, C., 2006. Temporal variations of *Q_c*-
511 1 and *b*-values associated to the December 2000–January 2001 volcanic activity at the
512 Popocatepetl volcano, Mexico. *Journal of Volcanology and Geothermal Research*, 251: 347-
513 358.

514 Patane, D., Caltabiano, T., Del Pezzo, E. and Gresta, S., 1992. Time variation of *B* and *Q_c* at Mt. Etna
515 (1981-87). *Physics of the Earth and Planetary Interiors*, 71: 137-140.

516 Power, J.A., Wyss, M. and Latchman, J.L., 1998. Spatial variations in the frequency-magnitude
517 distribution of earthquakes at Soufriere Hills Volcano, Montserrat, West Indies *Geophysical*
518 *Research Letters*, 29(19): 3652-3656.

519 Rydelek, P.A. and Sacks, I.S., 1989. Testing the completeness of earthquake catalogs and hypothesis of
520 self-similarity. *Nature*, 337: 251-253.

521 Sammonds, P.R., G., M.P. and Main, I.G., 1992. Role of pore fluids in the generation of seismic
522 precursors to shear fracture. *Nature*, 359: 228-230.

523 Sanchez, J.J., Gomez, J.A., Torres, P.A., Calvache, M.L., Ortega, A., Ponce, A.P., Acevedo, A.P., Gil-Cruz,
524 F., Londono, J.M., Rodriguez, S.P., Patino, J.D.J. and Bohorquez, O.P., 2005. Spatial mapping

525 of the b-value at Galeras volcano, Columbia, using earthquakes recorded from 1995 to 2002.
526 Earth Sci. Res. J., 9(1): 30-36.

527 Sanchez, J.J., McNutt, S.R., Power, J.A. and Wyss, M., 2004. Spatial Variations in the Frequency-
528 Magnitude Distribution of Earthquakes at Mount Pinatubo Volcano. Bullertin of Seismological
529 Society of America, 94(2): 430-438.

530 Scholz, C.H., 1968. The frequency-magnitude relation of microfracturing in rock and its relation to
531 earthquakes. BSSA, 58(1): 399-415.

532 Schorlemmer, D., Wiemer, S. and Wyss, M., 2005. Variations in earthquake-size distribution across
533 different stress regimes. Nature, 437(7058): 539-542.

534 Shi, Y. and Bolt, B.A., 1982. The standard error of the magnitude-frequency b value. Bulletin of the
535 Seismological Soceity of America, 72(5): 1677-1687.

536 Wiemer, S. and McNutt, S.R., 1997. Variations in the frequency-magnitude distribution with depth in
537 two volcanic areas: Mount St. Helens, Washington, and Mt. Spurr, Alaska. Geophysical
538 Research Letters, 24(2): 189-192.

539 Wiemer, S., McNutt, S.R. and Wyss, M., 1998. Temporal and three-dimensional spatial analyses of the
540 frequency–magnitude distribution near Long Valley Caldera, California. Geophys. J. I., 134:
541 409-421.

542 Wiemer, S. and Wyss, M., 2000. Minimum Magnitude of Completeness in Earthquake Catalogs:
543 Examples from Alaska, the Western United States, and Japan. Bulletin of the Seismological
544 Society of America, 90(4): 859-869.

545 Wiemer, S. and Wyss, M., 2002. Mapping spatial variability of the frequency-magnitude distribution
546 of earthquakes. Advances in Geophysics, 45: 259-302.

547 Woessner, J. and Wiemer, S., 2005. Assessing the Quality of Earthquake Catalogues: Estimating the
548 Magnitude of Completeness and Its Uncertainty. Bulletin of the Seismological Society of
549 America, 95(2): 684-698.

550 Wyss, M., Klein, F., Nagamine, K. and Wiemer, S., 2001. Anomalously high b-values in the South Flank
551 of Kilauea volcano, Hawaii: evidence for the distribution of magma below Kilauea's East rift
552 zone. Journal of Volcanology and Geothermal Research, 106: 23-37.

553 Wyss, M., Shimazaki, K. and Wiemer, S., 1997. Mapping active magma chambers by b values beneath
554 the off-Ito volcano, Japan. Journal of Geophysical Research, 102(B9): 20413-20422.

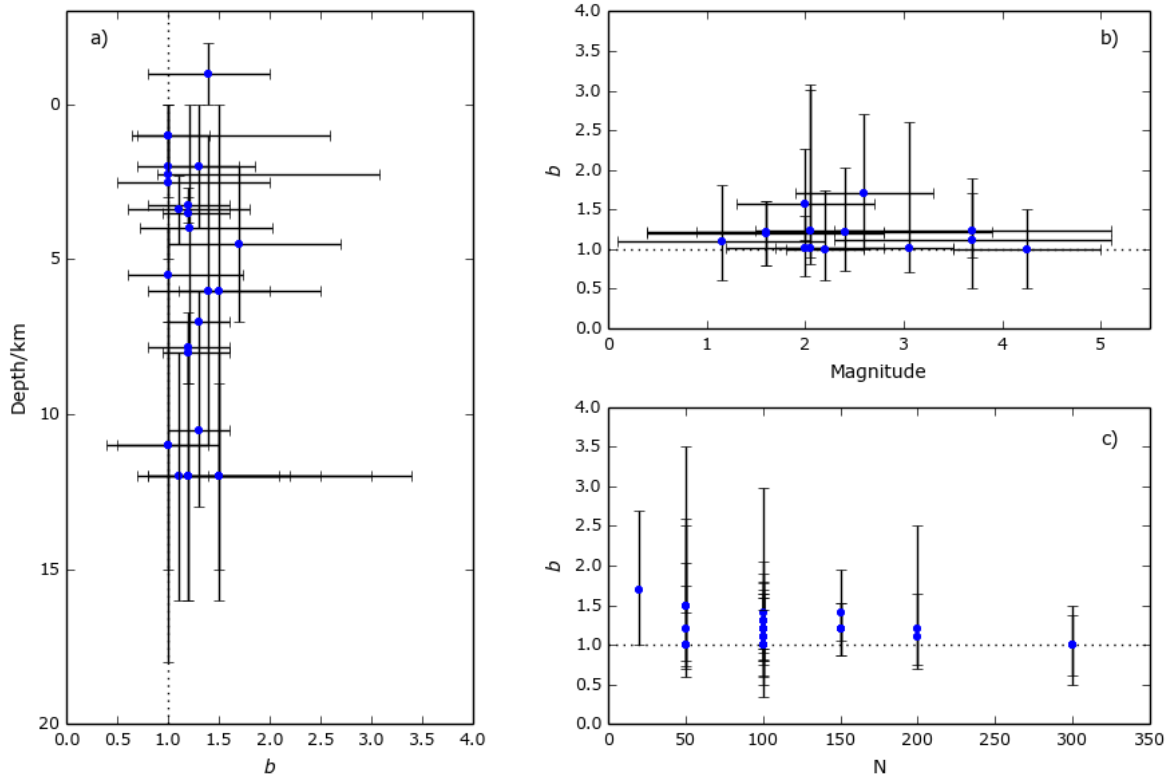
555

556

558 Table 1 - Compilation of *b*-values and range of magnitudes for volcanic seismic catalogues

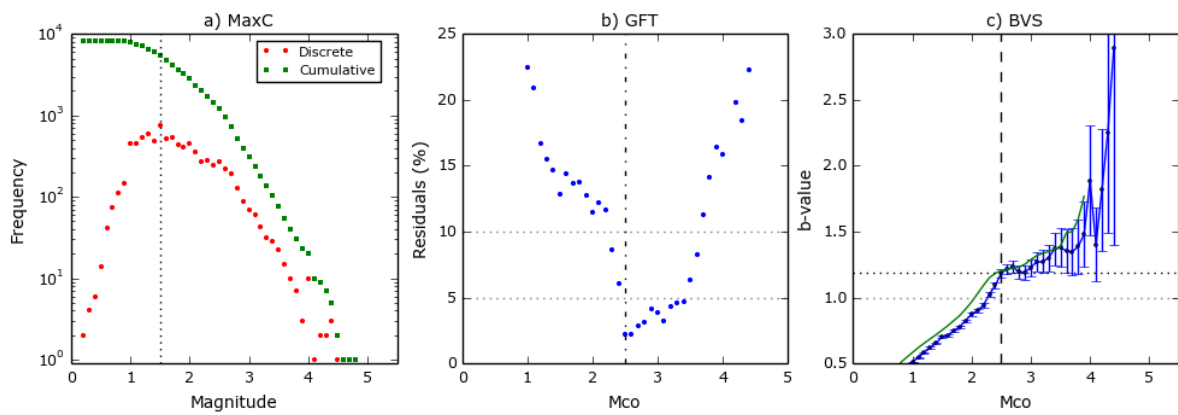
Reference	Volcano	Dates	Depth, km	<i>N</i>	Method <i>Mc</i>	Mag. range	Method <i>b</i>	<i>b</i> _{min}	<i>b</i> _{typ}	<i>b</i> _{max}
(Jacobs and McNutt, 2010)	Augustine	2000 - 2006	-2-0	100	ZMAP	-	MLE	0.8	1.4	2.1
(Jacobs and McNutt, 2010)	Augustine	17/11/05 - 10/12/05	-2-0	~250	ZMAP	-0.1-0.7	MLE	-	-	1.85
M. Wyss (written comm.)	Coso		0.8-3					-	-	1.7
(Ibanez et al., 2012)	El Hierro	19/7/11 - 16/9/11	8-16	7000+	90GFT	1.3-2.7	LS	1.12	1.57	2.25
(Ibanez et al., 2012)	El Hierro	19/07/2011	8-16	200	90GFT	-	LS	0.75	1.25	2.55
(Marti et al., 2013)	El Hierro	14/8/11 - 18/8/11	8-16	-	-	-	MLE	0.8	1.1	2.3
(Ibanez et al., 2012)	El Hierro	19/7/11 - 28/7/11	8-16	-	90GFT	1.5-2.6	LS	0.81	1.2	3.01
(Patane et al., 1992)	Etna	1984	-	200	-	2.8-	MLE	0.8	1.1	1.7
(Patane et al., 1992)	Etna	29/3/1983 - 6/8/1983	-	-	-	2.5-	MLE	0.7	1.0	2.1
(Murru et al., 1999)	Etna	-	9-15	50	MaxC	2.5-	MLE	1.4	1.5	3.5
(Centamore et al., 1999)	Etna	1/1/1990 - 31/12/92	-	100	-	2.3-5.1	LS	0.5	1.2	1.9
(Centamore et al., 1999)	Etna	1/1/1990- 31/12/92	-	100	-	2.3-5.1	MLE	0.9	1.1	1.7
(Murru et al., 2007).	Etna	July - Aug 2001	0-2	50	GFT	2.6-3.5	MLE	0.7	1	2.6
(Murru et al., 2005)	Etna	July - Aug 2001	0-12	50	90GFT	2.6	MLE	0.8	1.5	2.50
(Murru et al., 2007)	Etna	Aug 1999 - Dec 2005	1-3	100	90GFT	2.5	MLE	0.7	1.0	1.86
(Sanchez et al., 2005)	Galeras	Sep 1995 - Jun 2002	0-2	300	-	1.2-2.8	MLE	0.65	1.0	1.4
(Jolly and McNutt, 1999)	Katmai	-	6-8	-	-	-	-	1.0	1.3	1.6
(Wyss et al., 2001)	Kilauea	-	4-7,20	-	-	-	-	-	-	1.9
(Wyss et al., 2001)	Kilauea	1979 - 1997	4-7	50	-	1.8-2.6	MLE & LS	0.6	1.0	1.73
(Wiemer et al., 1998)	Long Valley	1989 - 1998	1-11	150	MaxC	1.3-	MLE	1.1	1.4	2.0
(Jolly and McNutt, 1999)	Mageik	Sep 1996 - April 1997	0-5	-	-	-	WLS	1.0	1.5	2.0
(Bridges and Gao, 2006)	Makushin	July 1996 - April 05	0-8	50	74GFT	0.9-3.9	MLE	0.73	1.21	2.03
(Wiemer et al., 1998)	Mammoth Mtn.	1989 - 1990.5	3-4,7-9	150	MaxC	1.3-	MLE	0.95	1.2	1.6
(Jolly and McNutt, 1999)	Martin/Mageik	Sep 1996 - April 1997	-2-10	-	-	0.7-4.5	WLS	-	-	1.56
(Wiemer and McNutt, 1997)	Mount Spurr	1991 - 1995	2.3-4.5	100	Inspection	0.1-2.2	MLE & LS	0.6	1.1	1.8
(Main, 1987)	Mount St Helens	20 Mar - 18May 1980	na	~300	Inspection	3.5-5	MLE	0.5	1.0	1.5
(Wiemer and McNutt, 1997)	Mount St. Helens	1988 - Jan 1996	2.7-3.8	100	Inspection	0.4-2.8	MLE & LS	0.8	1.2	1.6
(Wyss et al., 1997)	Off-Ito	1982 - 1996	7-15	100	MaxC	1.6-2.5	MLE	0.44	1.0	1.54
M. Wyss (written comm.)	Oshima		4					-	-	1.5
(Sanchez et al., 2004)	Pinatubo	29 June - 19 Aug 1999	0-4,8-13	100	ZMAP	0.73-	MLE	1.0	1.3	1.7
(Novelo-Casanova et al., 2006)	Popocatepetl	Dec 2000 - Jan 2001	2-7	20	Inspection	1.9-3.3	MLE	1.0	1.7	2.70
S. Wiemer (written. comm.)	Redoubt		3-4,6-8					-	-	1.7
(Power et al., 1998)	Soufriere Hills	Aug 1995 - Mar 1996	2.0-2.5	100	-	1.7-2.4	MLE	0.9	1	3.07
(Farrell et al., 2009)	Yellowstone	1984 - 2006	4-18	>10	EMR	1.5-	MLE	0.5	1.0	1.5

Values for *N* are the number of events analysed in each catalogue. These figures are either given or estimated from figures. The methods for calculating the completeness magnitude, *Mc*, are; using ZMAP software; the Goodness-of-Fit method (GFT) with given percentage threshold (e.g. 90Gft is 90% fit); the Maximum Curvature method (MaxC); Inspection is choosing a *Mc* by eye; and using the Entire Magnitude Range method (EMR). The methods for approximating the *b*-value are the Maximum Likelihood Estimation (MLE) and the Least Squares and Weighted Least Squares fit (LS & WLS). The *b*-value ranges in each study are described by the minimum (*b*_{min}) and maximum (*b*_{max}) quoted values in the study, with a typical value (*b*_{typ}) being estimated by eye.



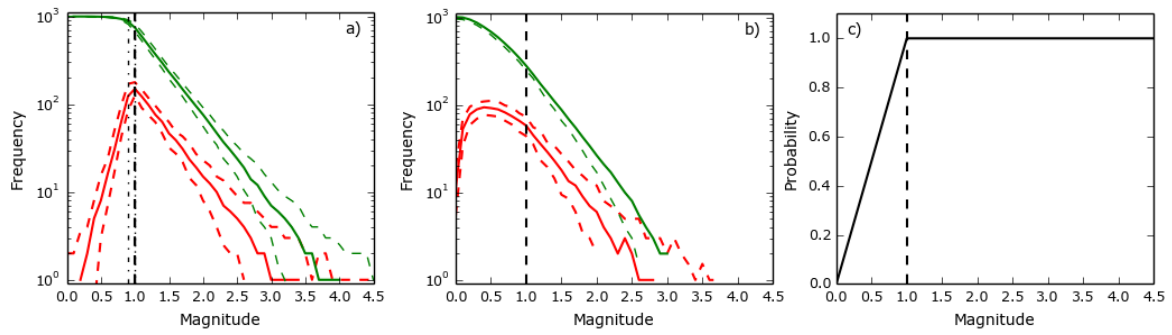
561

562 **Figure 1** – Synthesis of b -value distributions compared to a) depth, b) Magnitude, and c) the number of events in each
 563 catalogue, N . The errors bars show the minimum and maximum values of b from Table 1, and the range of depth/magnitude
 564 over which the catalogue was comprised. The blue dots show the typical b -values. Dotted line marks $b=1$.



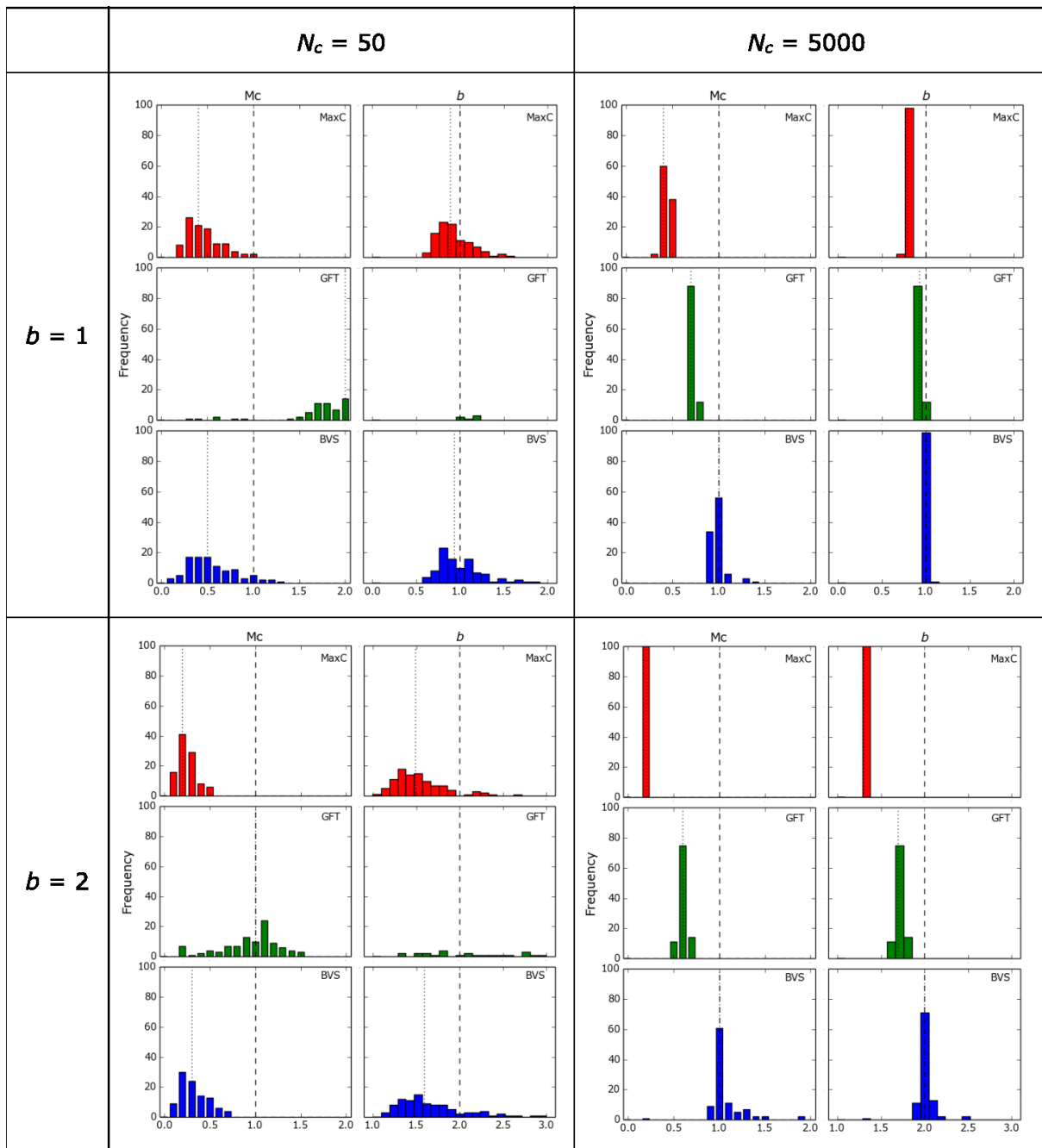
565

566 **Figure 2** – a) Discrete and cumulative frequency-magnitude distributions, demonstrating the Maximum Curvature Method
 567 (MaxC). The vertical dotted line represents the estimate of M_c at the highest discrete magnitude bin at ($M_c=1.5$). b) Residuals
 568 of the Goodness-of-Fit method (GFT) as a function of trial cut-off. Once the residual falls beneath 5% the completeness
 569 magnitude is selected, in this case $M_c=2.5$. c) b -value stability curve showing the b -values for each cut-off magnitude. The
 570 vertical dashed line indicates when successive b -values (green line) fall within error of the b -value. Here $M_c=2.5$.



571

572 **Figure 3** – a) Example of a sharp-peaked frequency-magnitude distribution. b) Example of a broad-peaked frequency-
 573 magnitude distribution. Both catalogues have an M_c of 1.0 and a b -value of 1.0. Discrete distributions are in reds, cumulative
 574 distributions are in green. The dashed lines show the 95% confidence intervals representing the scatter in the synthetic data
 575 c) The probability filter applied to b). Above $M_c=1.0$ all generated events are kept in the catalogue. Beneath $M_c=1.0$ there is
 576 a constantly decreasing probability that that will remain in the catalogue, creating the broad peak in the filtered discrete
 577 FMD.

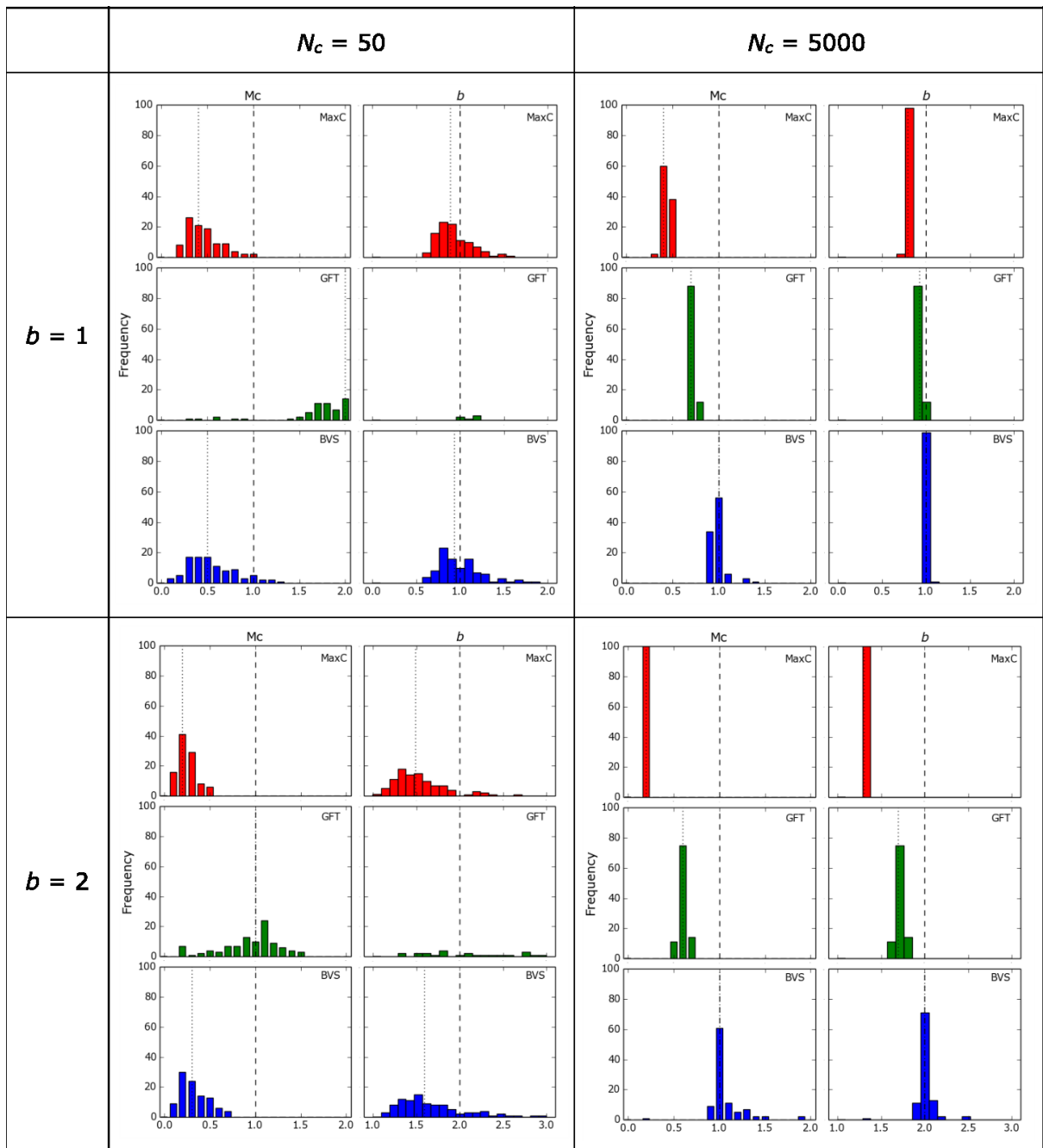


578

579 **Figure 4** – Histograms for the estimated Mc and b -value for the MaxC (red), GFT (green), and BVS (blue) methods for different
 580 catalogue sizes (columns) and b -values (rows) for the sharp-peaked distribution. The known values of $Mc=1.0$ and $b=1.0$ are
 581 marked with vertical bold dashed lines. The median value calculated by each method is shown by the vertical dotted line.

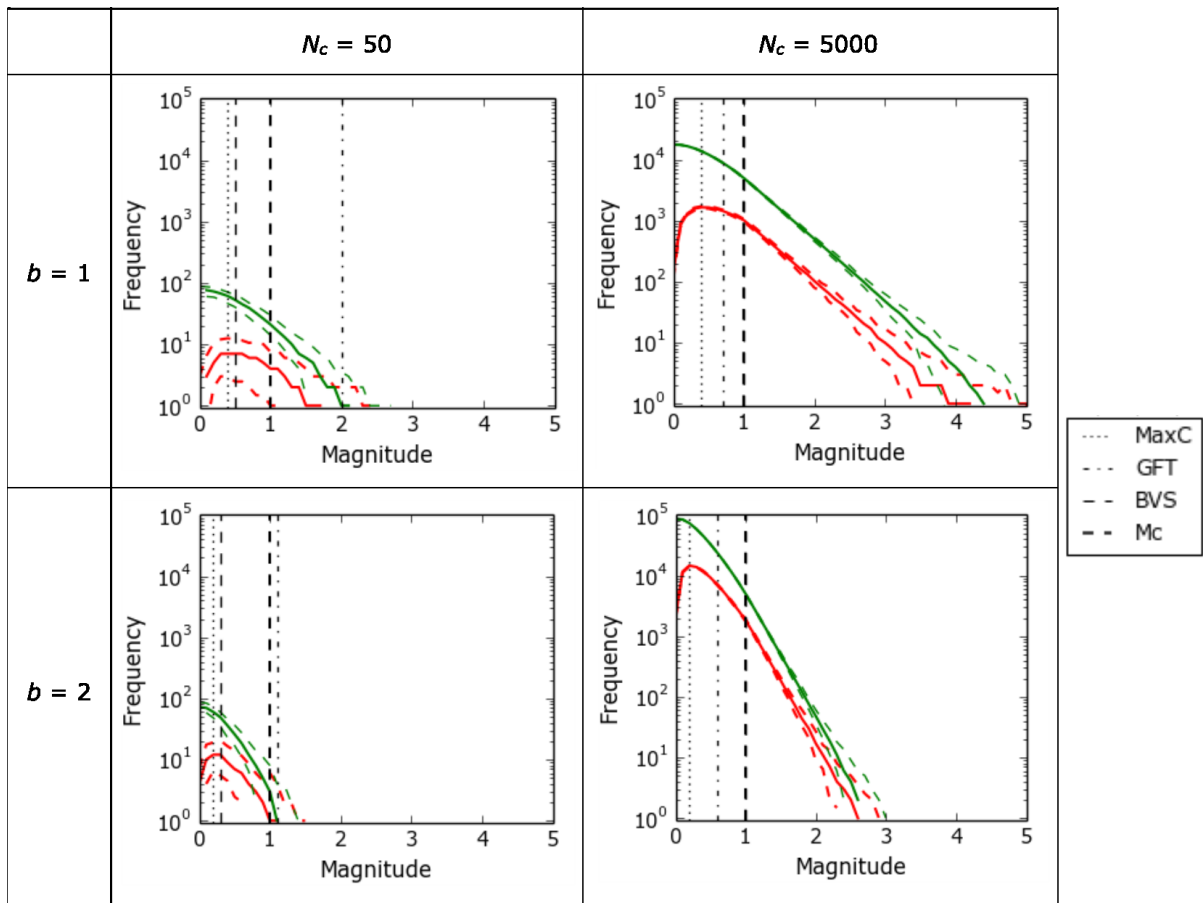
582

583



584

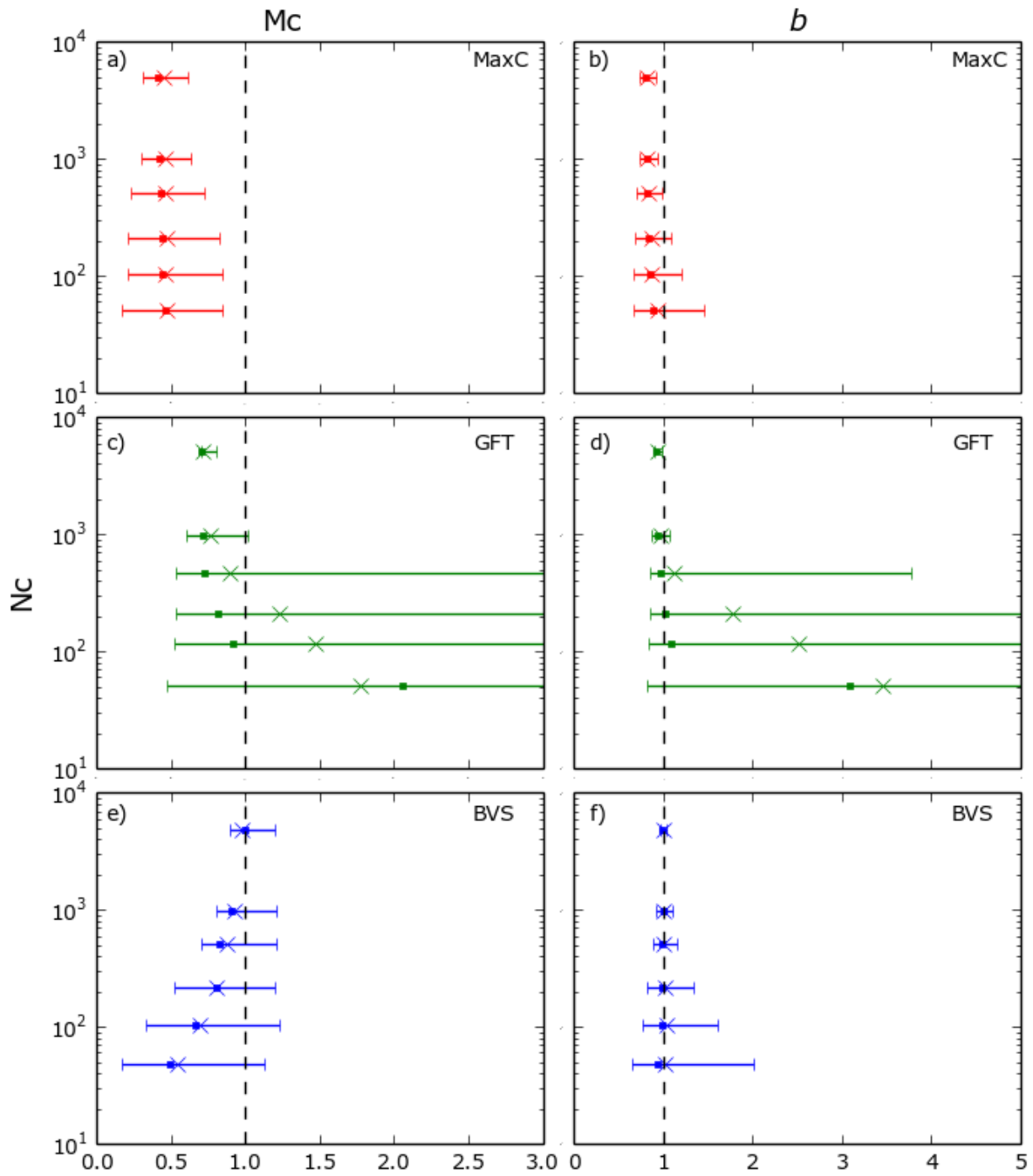
585 **Figure 5** – Histograms as in Figure 4 except for a broad-peaked distribution.



586

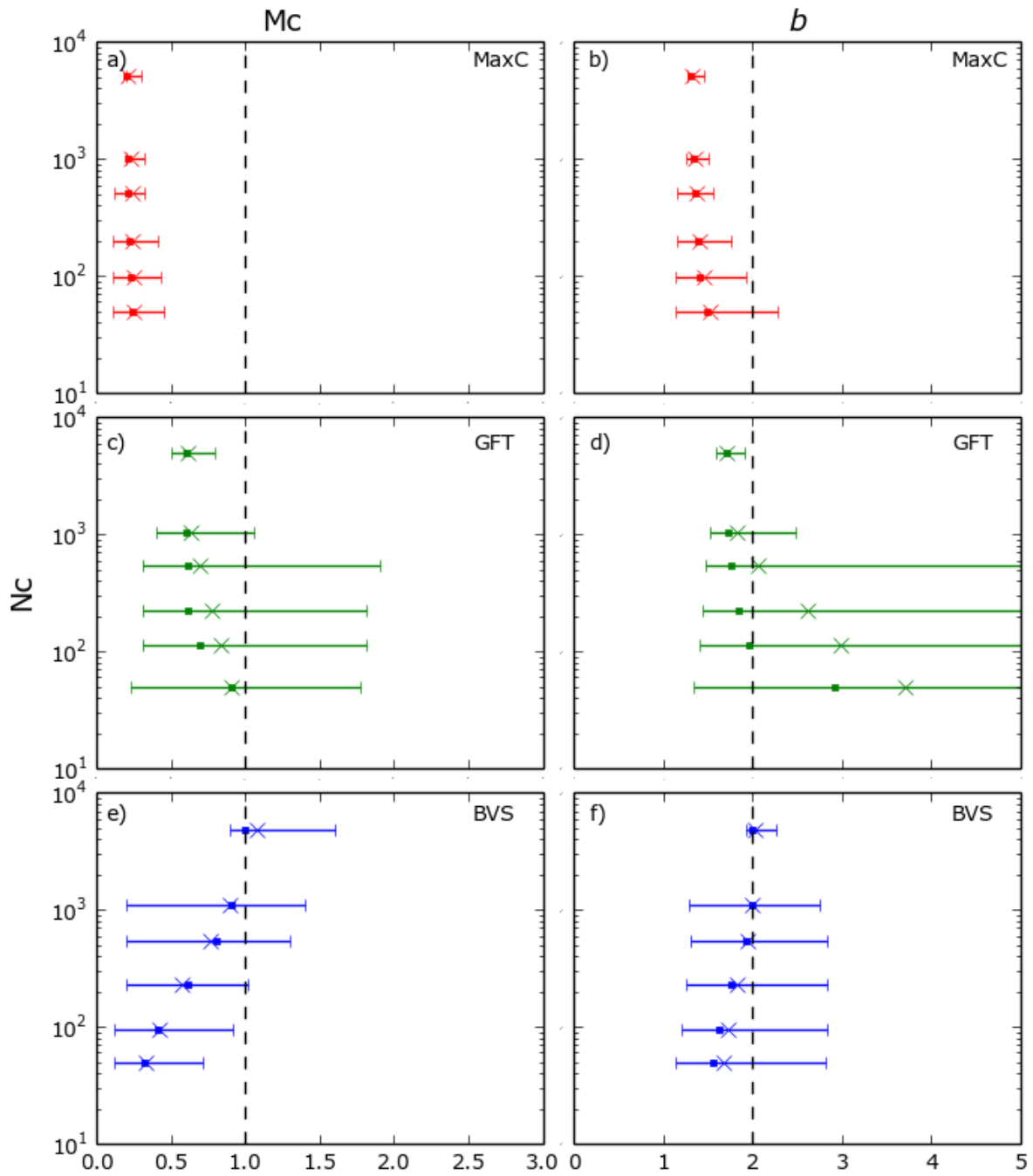
587 **Figure 6** – Frequency-magnitude distributions for $b=1$ & 2, and $N_c=50$ & 5000 in the case of a broad-peaked distribution. Red
 588 shows discrete frequency and green cumulative frequency. The solid red and green lines show the average values of the 100
 589 catalogues. The dashed lines represent a 95% confidence window. The vertical dashed black lines show the known Mc of the
 590 catalogue, $Mc=1.0$, and the Mc 's calculated by each method.

591



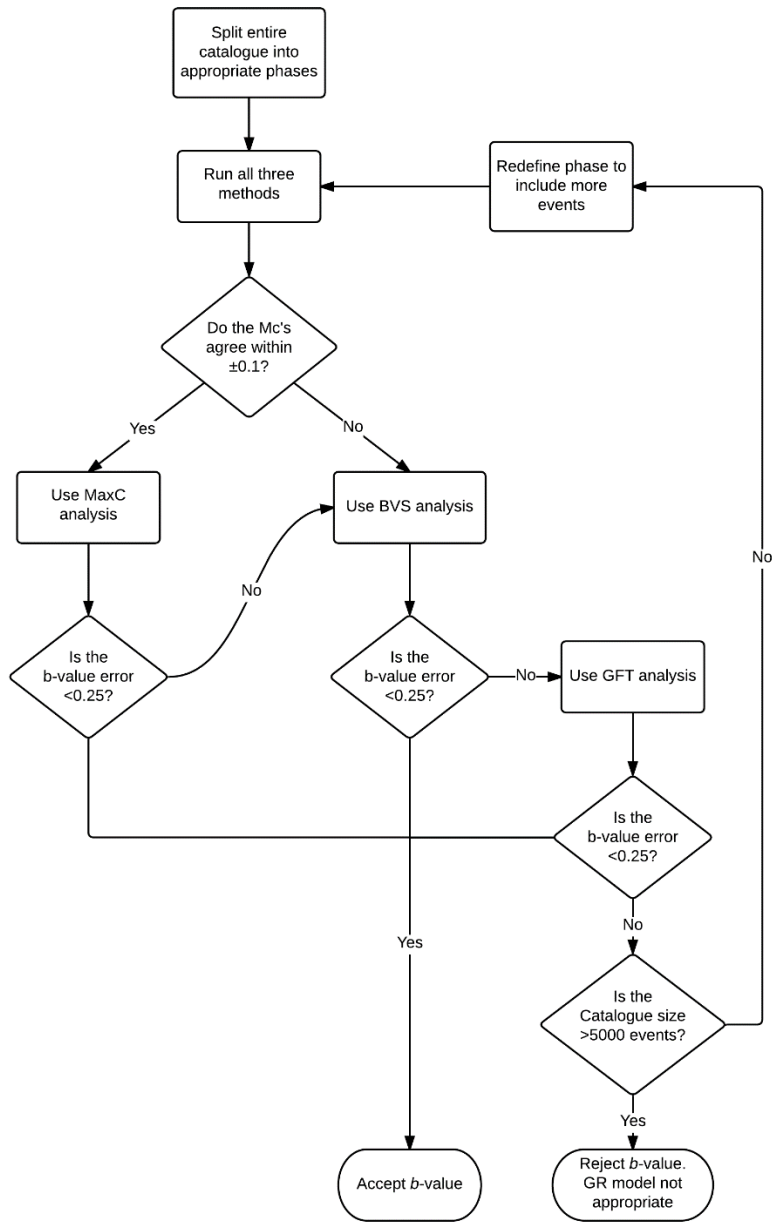
592

593 **Figure 7** - Summary of histograms for broad-peaked distributions in Figure 5 for $b=1$. They show the spread of Mc 's and b -
 594 value's against catalogue size, N , for each of the three methods. Error bars represent a 95% spread of the data, with dots
 595 representing the median value and x's the average. The known $Mc=1.0$ and $b=1.0$ are marked with a vertical dashed line.



596

597 **Figure 8** - Summary graphs as in Figure 7 but for $b=2$.

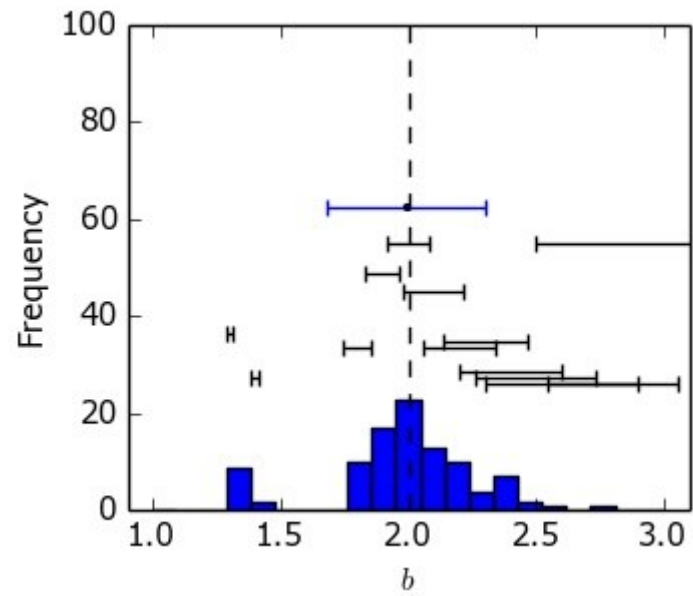


598

599

600

Figure 9 - Proposed workflow for best practice based on synthetic analysis.



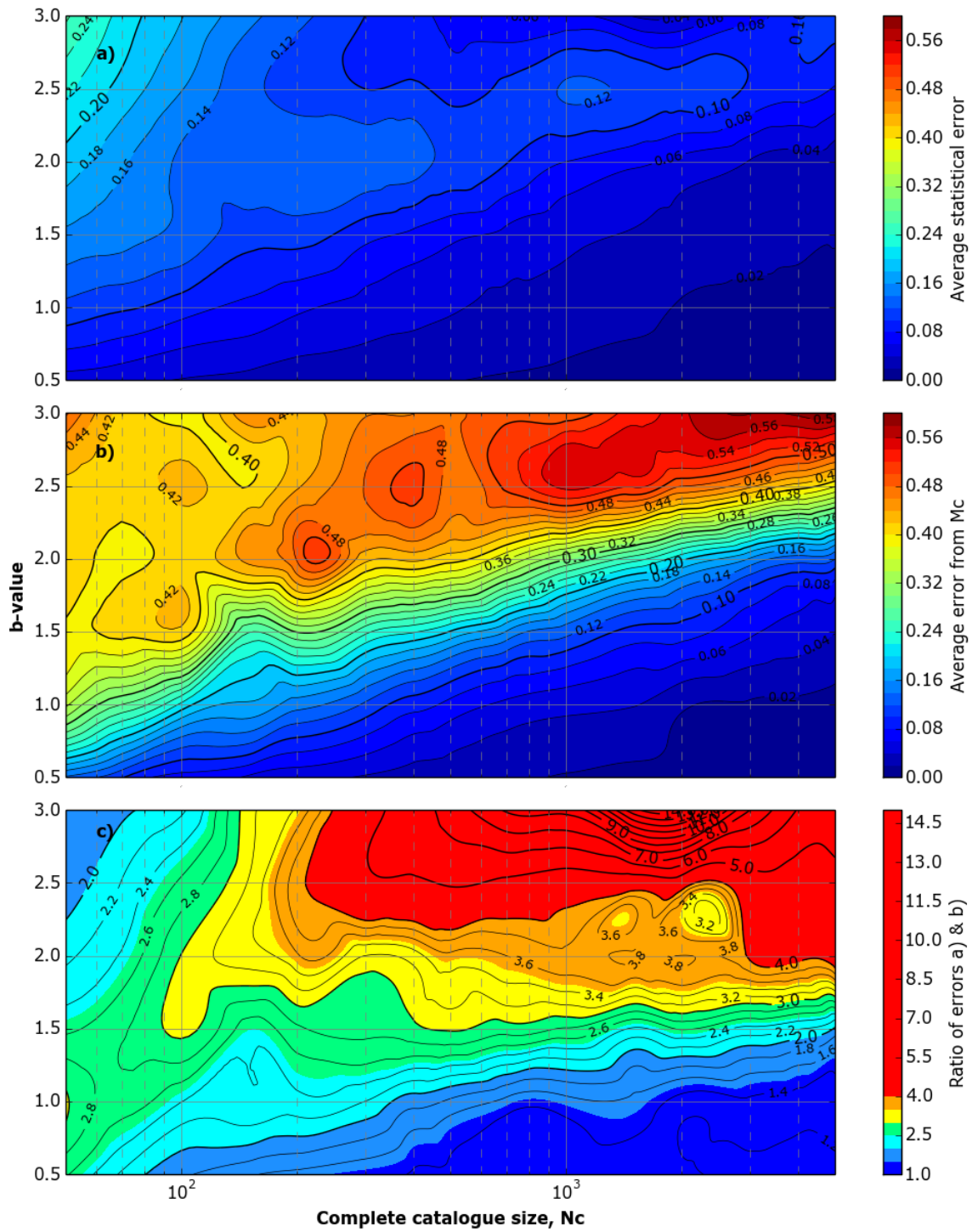
601

602

603

604

Figure 10 - b -value frequency plot for 100 synthetic catalogues when $N_c=1000$ and $b=2$. The blue (epistemic) error bar represents one standard deviation error in the data centred on the median b -value. The black error bars show the average aleatoric (Shi & Bolt b -value uncertainty) error for each bin.



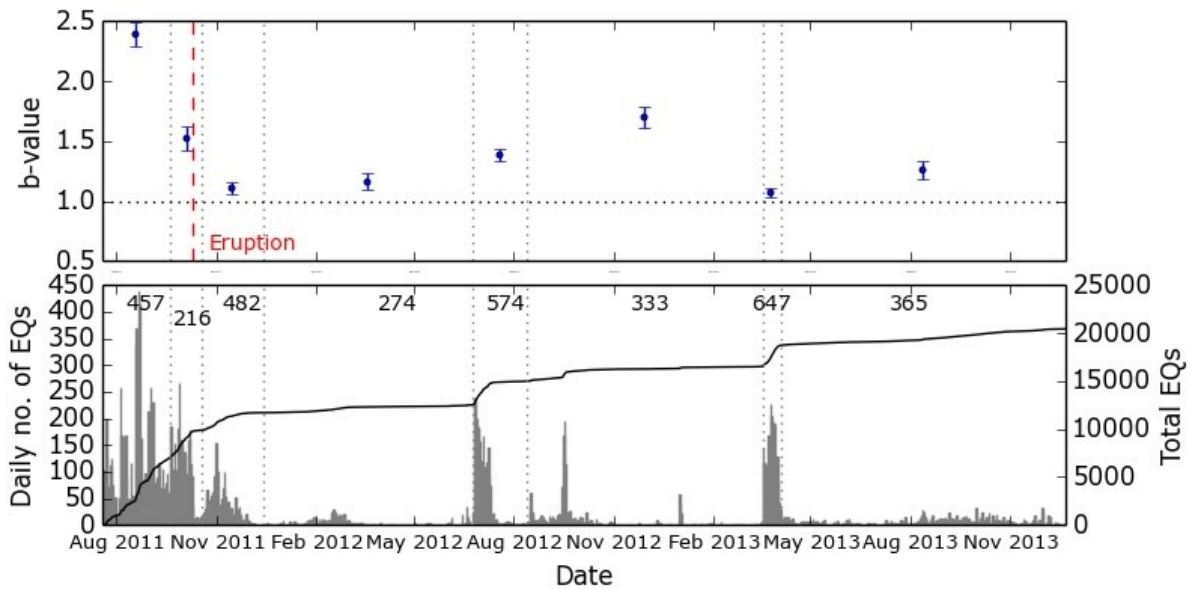
605

606

607

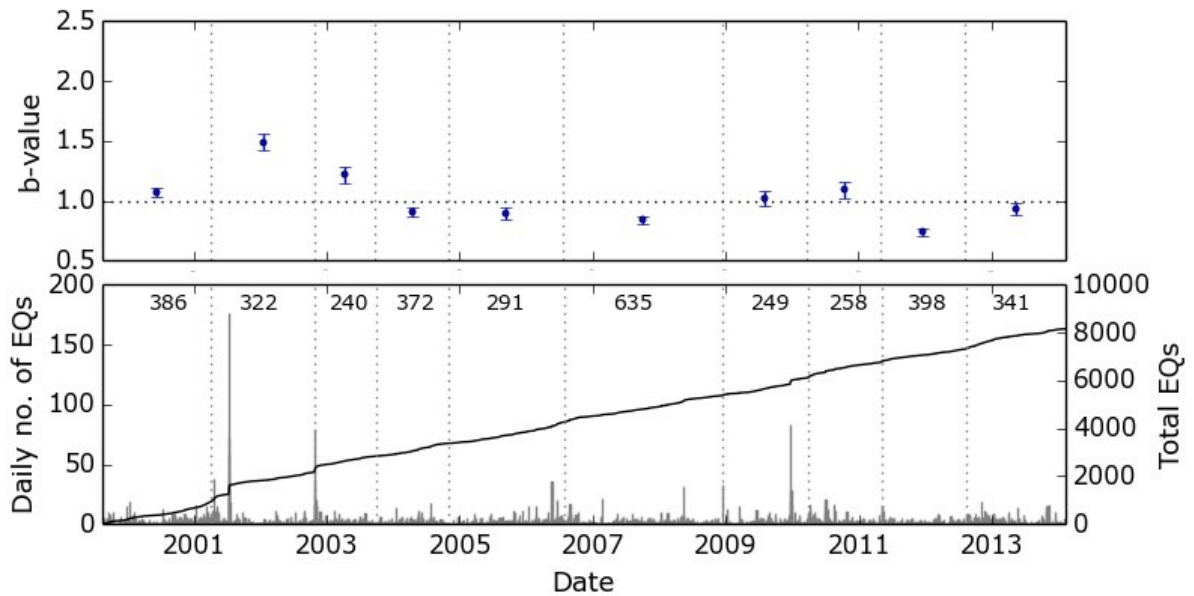
608

Figure 11 – Contour plots showing a) the statistical error in b -value estimated from eq. (5) as a function of varying complete catalogue size, N_c , and b -value. b) The error in b -value associated with the uncertainty in calculating M_c , estimated as in the example given in Fig 10 as a blue horizontal error bar c) The ratio of the error in (b) to the statistical error in (a).



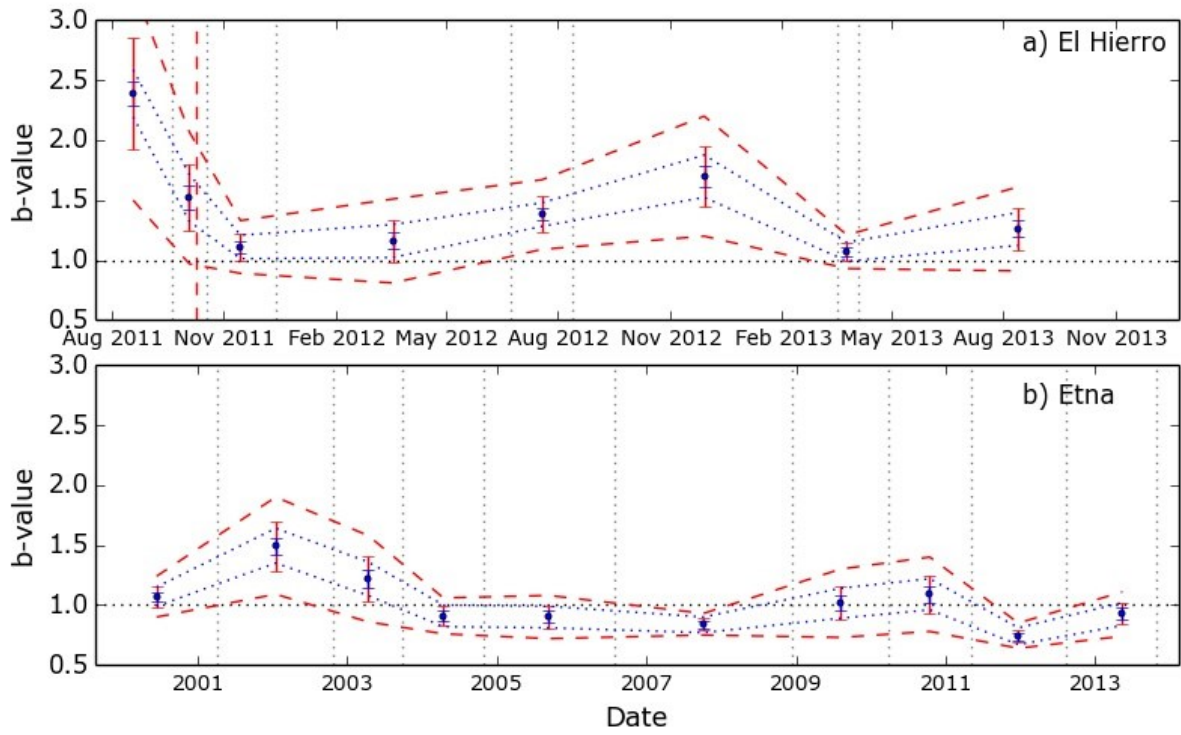
609

610 **Figure 12** – Top: *b*-value variation through time for the July 2011 to December 2013 El Hierro seismic catalogue using the
 611 proposed workflow. The eruption date is marked by the red dashed line. Bottom: Daily number of events (grey bars) and
 612 cumulative number of events (black line). The phase divisions are marked by vertical grey dotted lines with the number of
 613 events in the complete catalogue of each phase noted at the top of the plot.



614

615 **Figure 13** – Plots as in Figure 12 but for the 1999 - 2014 Mount Etna seismic catalogue.



616

617 **Figure 14** - *b*-value variation through time for a) the 2011-13 El Hierro catalogue, and b) the 1999 - 2014 Mount Etna seismic
 618 catalogue. Sample bias errors in are blue and estimated epistemic error are in grey. One standard deviation error is
 619 represented by the error bars and the grey dashed and blue dotted line respectively represent the 2 standard deviation error
 620 envelope.

621